Letter

Origin of the spin-crossover phenomenon in LaCoO₃

K. Katsumata ●

45-11 Kumanocho, Itabashi, Tokyo 173-0025, Japan

The origin of the spin-crossover phenomenon in LaCoO₃ is discussed based on the electronic state ^5D realized in a $3d^6$ system subjected to an intermediate crystal field. We calculate the splitting of the ^5D state under a crystal field whose symmetry is predominantly cubic but with a trigonal distortion. We confine ourselves to the Γ_5 state and use a fictitious orbital angular momentum $\boldsymbol{l}$ of magnitude one. Eigenvalues of a Hamiltonian including the spin-orbit interaction $-\lambda' \boldsymbol{l} \cdot \boldsymbol{S}$ and the trigonal crystal fields $9B_2^0(l_z^2 - 2/3) - 80B_4^0(l_z^2 - 9/10)$ are rigorously calculated. A singlet ground state with an energy gap to the excited states is realized for certain values of the parameters in the Hamiltonian. The magnetization calculated rigorously using the energy levels subject to a magnetic field accords with published measurements.

The compound LaCoO₃ (abbreviated LCO) has attracted much attention because of its possibly unique magnetic and electrical properties [1]. It shows a transition from a metallic to semiconducting state in the vicinity of 500 K, together with an anomaly in the magnetic susceptibility χ [2].

An interesting phenomenon awaiting a satisfactory explanation emerges in χ at lower temperatures. The magnetic susceptibility increases with decreasing temperature and is at a maximum in the neighborhood of 100 K [3]. Thereafter, χ decreases with decreasing temperature and begins to increase again at about 35 K [3]. Since the increase in χ below ∼35 K comes from magnetic impurities [4], LCO is considered to be in a nonmagnetic state at low temperatures, apart from the temperature-independent paramagnetism found in the nuclear magnetic resonance measurements [4].

Several attempts to interpret the origin of the transition from the nonmagnetic to magnetized states at a temperature ≃100 K, named the spin-crossover phenomenon, have been made [1]. To begin with, $3d$ orbital states of a trivalent cobalt ion ($3d^6$) in an octahedral crystal field split into a lower triplet (Γ_5 symmetry type) and upper doublet (Γ_3). In the case of a strong crystal field [5], the six $3d$ electrons are accommodated in the Γ_5 state with three up- and three down-spins, resulting in a nonmagnetic state. In an intermediate crystal field [5], however, Hund's rules predominate and the ground state of a $3d^6$ system is a ^5D with a total angular momentum $L = 2$ and total spin $S = 2$ [5].

Most interpretations on the origin of the spin-crossover phenomenon have used the first scenario mentioned above. Progress to a plausible model requires intermediate-spin (IS) and high-spin (HS) states, in addition to the nonmagnetic [low-spin (LS)] one, to explain the temperature-dependent magnetism of LCO [1]. There is no consensus on which combinations of LS, IS, and HS states best describe the magnetic properties of LCO. In this Letter, we present an interpretation based on the second scenario for $3d$ states that possesses many attractive features, not least its relative simplicity.

Inomata and Oguchi (IO) calculated [6] the magnetic properties of FeCl₂ · 2H₂O with a crystal field of intermediate strength, and their findings apply to LCO since the ferrous ion Fe^{2+} and Co^{3+} possess the atomic configuration $3d^6$. A ^5D state splits into Γ_5 and Γ_3 with an energy separation, typically ∼10^4 cm⁻¹ in an octahedral crystal field [5], much larger than room temperature (300 K ≃ 200 cm⁻¹). Within the assumed Γ_5 ground state we may use a fictitious orbital angular momentum $\boldsymbol{l}$ of magnitude one [7,8] related to the total angular momentum $\boldsymbol{L}$ by [8]

$$\boldsymbol{L} = -\boldsymbol{l}. \tag{1}$$

The corresponding effective ^5D Hamiltonian [6]

$$\mathcal{H}_{\text{IO}} = -\lambda' \boldsymbol{l} \cdot \boldsymbol{S} - \Delta(l_z^2 - 2/3) \tag{2}$$

includes spin-orbit coupling and a tetragonal distortion with strengths λ' and Δ, respectively. Although not stated explicitly, IO have shown [6] the possibility of a singlet ground state with an energy gap to excited states for a ^5D system under a tetragonal crystal field. Likewise, Kadwański and Ropka [9] made a computer calculation on a ^5D system subjected to a crystal field and realized a singlet ground state.

The crystal structure of LCO is rhombohedral with space group $R\bar{3}c$ below room temperature [10]. Bull and Knight [11] performed a high-resolution neutron diffraction measurement on this material. Their results show that with decreasing temperature the CoO₆ octahedra rotate about the rhombohedral [111] axis, and that the octahedra are distorted. In the following, we calculate the splitting of the ^5D state under a crystal field whose symmetry is predominantly cubic but with a trigonal distortion. The Hamiltonian describing the crystal field of trigonal symmetry is given by [5]

$$\mathcal{H}_{\text{crys}} = B_2^0 O_2^0 + B_4^0 O_4^0, \tag{3}$$

where B_2^0 and B_4^0 are the magnitudes of the crystal field and O_2^0 and O_4^0 are the equivalent operators. Here, the axis of

quantization z is taken parallel to a line drawn from the center through the midpoint of one of the faces of the octahedron [5].

The basis functions belonging to the Γ_5 state are given by [5]

$$|\tilde{1}\rangle = \sqrt{1/3}\{\sqrt{2}|-2\rangle - |1\rangle\}, \tag{4}$$

$$|\tilde{0}\rangle = |0\rangle, \tag{5}$$

and

$$|-\tilde{1}\rangle = -\sqrt{1/3}\{\sqrt{2}|2\rangle + |-1\rangle\}. \tag{6}$$

For the Γ_3 state, the basis functions are

$$|\tilde{+}\rangle = \sqrt{1/3}\{|-2\rangle + \sqrt{2}|1\rangle\}, \tag{7}$$

and

$$|\tilde{-}\rangle = \sqrt{1/3}\{|2\rangle - \sqrt{2}|-1\rangle\}. \tag{8}$$

In Eqs. (4)–(8), $|2\rangle$, $|1\rangle$, $|0\rangle$, $|-1\rangle$, and $|-2\rangle$ are the basis functions belonging to the ^5D state. These two sets of basis functions are related by the following transformation R,

$$R = \begin{pmatrix} 0 & -\sqrt{1/3} & 0 & 0 & \sqrt{2/3} \\ 0 & 0 & 1 & 0 & 0 \\ -\sqrt{2/3} & 0 & 0 & -\sqrt{1/3} & 0 \\ 0 & \sqrt{2/3} & 0 & 0 & \sqrt{1/3} \\ \sqrt{1/3} & 0 & 0 & -\sqrt{2/3} & 0 \end{pmatrix}. \tag{9}$$

The z component of $\boldsymbol{L}$ transforms as

$$RL_zR^{-1} = \begin{pmatrix} -1 & 0 & 0 & -\sqrt{2} & 0 \\ 0 & 0 & 0 & 0 & 0 \\ 0 & 0 & 1 & 0 & -\sqrt{2} \\ -\sqrt{2} & 0 & 0 & 0 & 0 \\ 0 & 0 & -\sqrt{2} & 0 & 0 \end{pmatrix}. \tag{10}$$

The matrix elements for L^+ and L^- are obtained similarly. The upper left 3×3 submatrix in Eq. (10) belongs to the Γ_5 representation, which results in Eq. (1). The lower right 2×2 submatrix belongs to the Γ_3. We see that the elements of this 2×2 submatrix are zero. This means that the orbital moment exists predominantly in the Γ_5 state. Therefore, we may assume that the spin-orbit interaction energy $\langle \lambda \boldsymbol{L} \cdot \boldsymbol{S} \rangle$ between the real orbital moment and spin is the same as that in the Γ_5 state given by $\langle -\lambda' \boldsymbol{l} \cdot \boldsymbol{S} \rangle$. The maximum value of $\langle \lambda \boldsymbol{L} \cdot \boldsymbol{S} \rangle$ is given for $L_z = 2$ and $S_z = 2$ resulting in $\langle \lambda \boldsymbol{L} \cdot \boldsymbol{S} \rangle = 4\lambda$. Similarly, the maximum value of $\langle -\lambda' \boldsymbol{l} \cdot \boldsymbol{S} \rangle$ is $2\lambda'$ when $l_z = -1$ and $S_z = 2$. From this consideration, we have

$$4\lambda = 2\lambda'. \tag{11}$$

The matrix elements of O_2^0 and O_4^0 in Eq. (3) are given in [5]. These operators transform as

$$RO_2^0R^{-1} = R\begin{pmatrix} 6 & 0 & 0 & 0 & 0 \\ 0 & -3 & 0 & 0 & 0 \\ 0 & 0 & -6 & 0 & 0 \\ 0 & 0 & 0 & -3 & 0 \\ 0 & 0 & 0 & 0 & 6 \end{pmatrix}R^{-1}$$

$$= \begin{pmatrix} 3 & 0 & 0 & 3\sqrt{2} & 0 \\ 0 & -6 & 0 & 0 & 0 \\ 0 & 0 & 3 & 0 & -3\sqrt{2} \\ 3\sqrt{2} & 0 & 0 & 0 & 0 \\ 0 & 0 & -3\sqrt{2} & 0 & 0 \end{pmatrix} \tag{12}$$

and

$$RO_4^0R^{-1} = R\begin{pmatrix} 12 & 0 & 0 & 0 & 0 \\ 0 & -48 & 0 & 0 & 0 \\ 0 & 0 & 72 & 0 & 0 \\ 0 & 0 & 0 & -48 & 0 \\ 0 & 0 & 0 & 0 & 12 \end{pmatrix}R^{-1}$$

$$= \begin{pmatrix} -8 & 0 & 0 & 20\sqrt{2} & 0 \\ 0 & 72 & 0 & 0 & 0 \\ 0 & 0 & -8 & 0 & -20\sqrt{2} \\ 20\sqrt{2} & 0 & 0 & -28 & 0 \\ 0 & 0 & -20\sqrt{2} & 0 & -28 \end{pmatrix}. \tag{13}$$

We see from Eqs. (12) and (13) that we may write the crystal field Hamiltonian Eq. (3) in an operator form as

$$\mathcal{H}_{\text{crys}} = 9B_2^0(l_z^2 - 2/3) - 80B_4^0(l_z^2 - 9/10). \tag{14}$$

The total Hamiltonian $\mathcal{H}$ we study here is given by

$$\mathcal{H} = -\lambda' \boldsymbol{l} \cdot \boldsymbol{S} + 9B_2^0(l_z^2 - 2/3) - 80B_4^0(l_z^2 - 9/10). \tag{15}$$

Since $l_z + S_z$ commutes with the Hamiltonian [Eq. (15)], its eigenvalue m can be used to classify the states. We denote the states by $|l_z, S_z\rangle$, where l_z and S_z take three and five states, respectively.

For $m = 3$,

$$E_3 = \langle 1, 2|\mathcal{H}|1, 2\rangle = -2\lambda' + \delta - \varepsilon, \tag{16}$$

where $\delta \equiv 3B_2^0$ and $\varepsilon \equiv 8B_4^0$.

The next eigenstate, $m = 2$, is a linear combination of $|1, 1\rangle$ and $|0, 2\rangle$. In this case, we have a 2×2 secular determinant from which we obtain

$$E_2 = -\lambda'/2 - \delta/2 + 4\varepsilon$$
$$\pm \frac{1}{2}\sqrt{9(\lambda')^2 - 6\lambda'\delta + 20\lambda'\varepsilon + 9\delta^2 - 60\delta\varepsilon + 100\varepsilon^2}. \tag{17}$$

When $m = 1$, we have the following cubic equation for the eigenvalues E_1,

$$E_1^3 - (2\lambda' + 7\varepsilon)E_1^2$$
$$- \{3\delta^2 + 17\varepsilon^2 + 5(\lambda')^2 - 20\delta\varepsilon + 2\delta\lambda' - 16\varepsilon\lambda'\}E_1$$
$$+ \{4\delta^2\lambda' - 22\delta\varepsilon\lambda' + 18\varepsilon^2\lambda' + 6(\lambda')^3 + 2\delta^3 - 13\delta^2\varepsilon$$
$$+ 20\delta\varepsilon^2 + 5\delta(\lambda')^2 - 5\varepsilon(\lambda')^2 - 9\varepsilon^3\} = 0. \tag{18}$$

The solutions of Eq. (18) are obtained with *Mathematica* in an analytical form. Lastly, the $m = 0$ state is a linear combination of $|1, -1\rangle$, $|0, 0\rangle$ and $|-1, 1\rangle$ with values

$$E_0 = \lambda' + \delta - \varepsilon, \tag{19}$$
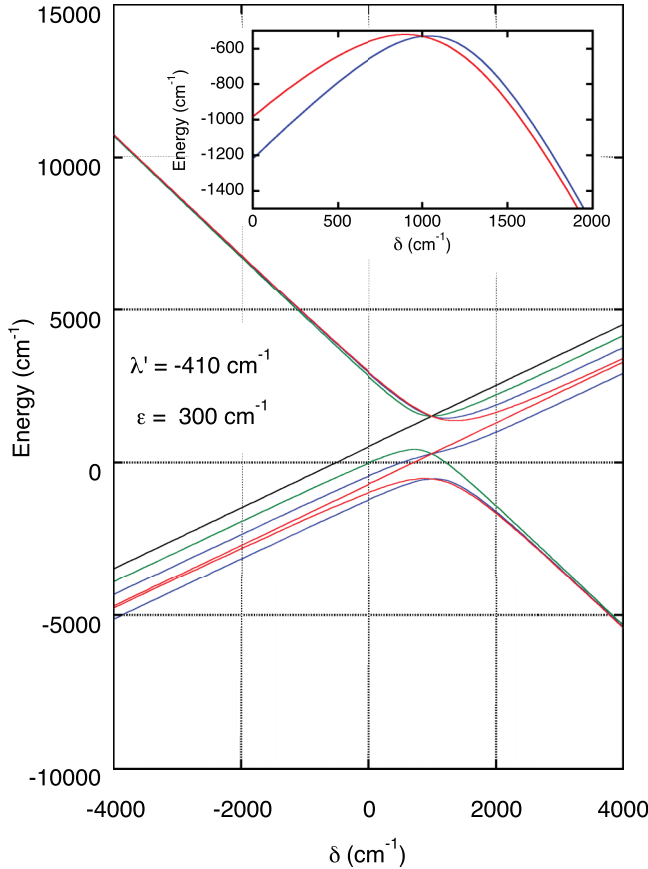
FIG. 1. The eigenvalues of the Hamiltonian [Eq. (15)] are plotted vs $\delta(\equiv 3B_2^0)$ when $\lambda' = -410$ cm^{-1} and $\varepsilon(\equiv 8B_4^0) = 300$ cm^{-1}. Black: $m = \pm 3$. Green: $m = \pm 2$. Blue: $m = \pm 1$. Red: $m = 0$. The inset shows the δ dependence of the lowest- and second lowest-energy levels.

and

$$E_0 = \lambda'/2 - \delta/2 + 4\varepsilon$$
$$\pm \frac{1}{2}\sqrt{25(\lambda')^2 + 9\delta^2 - 60\delta\varepsilon + 6\delta\lambda' + 100\varepsilon^2 - 20\varepsilon\lambda'}.$$

$$(20)$$

Similarly, we obtain the eigenvalues for $m = -1, -2,$ and -3.

The main panel of Fig. 1 shows the 15 eigenvalues of the Hamiltonian [Eq. (15)] as a function of δ when $\lambda' = -410$ cm^{-1} and $\varepsilon = 300$ cm^{-1}. The inset of Fig. 1 depicts the lowest- and second lowest-energy levels as a function of δ. We see that the ground state is a singlet ($m = 0$) with an energy gap to the first excited state for $\delta > 1000$ cm^{-1}.

Next, we calculate the magnetization M of LCO and compare the result with experiment. For this purpose, we calculate the eigenvalues under an applied magnetic field. We add the Zeeman Hamiltonian $\mathcal{H}_Z$,

$$\mathcal{H}_Z = \mu_B \boldsymbol{H}(2\boldsymbol{S} - \boldsymbol{l}), \qquad (21)$$

to Eq. (15), where μ_B is the Bohr magneton and $\boldsymbol{H}$ is the applied magnetic field. In this Letter, we consider the case of $\boldsymbol{H} \parallel z$.
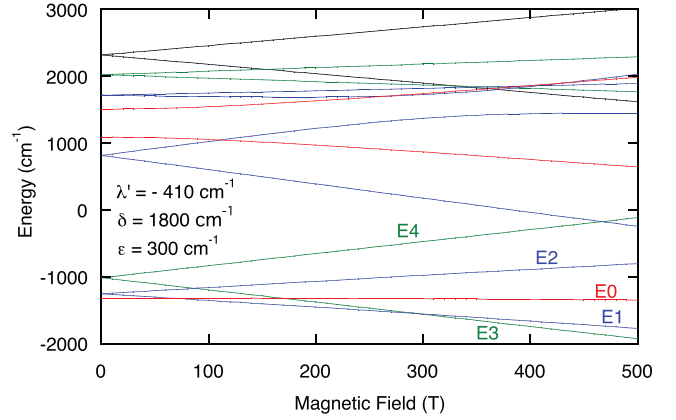

FIG. 2. The magnetic field dependence of the 15 eigenvalues when $\lambda' = -410$ cm^{-1}, $\delta(\equiv 3B_2^0) = 1800$ cm^{-1}, and $\varepsilon(\equiv 8B_4^0) = 300$ cm^{-1}. Black: $m = \pm 3$. Green: $m = \pm 2$. Blue: $m = \pm 1$. Red: $m = 0$.

We show in Fig. 2 the 15 energy levels as a function of the applied magnetic field. As is seen in Fig. 2, the energy levels named E_0 through E_4 lie about a few hundreds cm^{-1} below the higher-energy levels. Therefore, we may take only the low-lying five states to calculate M at low temperatures.

The calculation of M has been performed with the standard procedure of statistical mechanics. The partition function Z for the five states is formulated from which the free energy F is obtained. Then the derivative of F is calculated with respect to H to obtain M. The expression for M is lengthy and so we do not present it here.

We compare the results of our calculation with the experiment reported by Sato *et al.* [12]. The experimental data are extracted [13] from Fig. 1 of [12]. The inset of Fig. 3 shows the theoretical and experimental data. Here, we assume that all the Co ions in the sample are in the ^5D state ($p = 1.0$). In this case, the agreement between theory and experiment is not good.
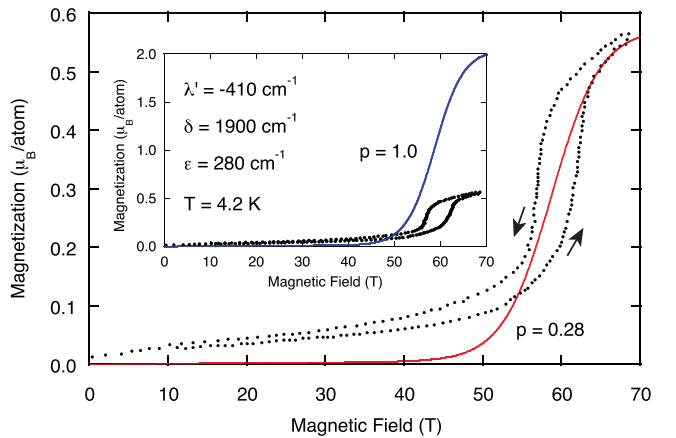

FIG. 3. The magnetic field dependence of the magnetization of LaCoO$_3$ at $T = 4.2$ K. Red curve: Theory with the concentration $p = 0.28$ of Co atoms in the ^5D state. Black dots: Experimental result reported by Sato *et al.* [12]. The experimental data are extracted [13] from Fig. 1 of [12]. The inset shows the theoretical curve with $p = 1.0$ and the experimental data.

Not all Co ions in LCO are in the ^5D state according to results for $p = 1.0$ presented in Fig. 3, and independent information supports this finding. Goodenough [14] pointed out that trivalent cobalt under an octahedral crystal field has a low-spin (Co^{III}) and a high-spin (Co^{3+}) state of comparable energy. This suggests that Co^{III} and Co^{3+} coexist in LCO. From a Mössbauer study on LCO, Bhide *et al.* [15] showed that at low temperatures, cobalt ions exist predominantly in the Co^{III} state and they transform partially to Co^{3+} ions up to 200 K.

We show in the main panel of Fig. 3 the theoretical curve with the Co^{3+} concentration $p = 0.28$ together with the experimental data [12]. Here, we have assumed that Co^{III} ions are magnetically silent at low temperatures. The agreement between theory and experiment is satisfactory. The magnetization we calculate here is the one at thermal equilibrium. So, the hysteretic behavior seen in the pulsed field measurement is not reproduced. The equilibrium value is considered to lie between the data taken in increasing and decreasing fields.

The slope in the field dependence of magnetization observed at low fields originates from the temperature-independent paramagnetic susceptibility [4], not from magnetic impurities. If the slope were due to impurities, its magnetization saturates at a moderate field following the Brillouin function and would give a field-independent value. The temperature-independent susceptibility originates from the contribution of higher-energy levels [16]. As explained above, we have considered the five low-lying energy levels in our calculation. A calculation including the higher-energy levels will reproduce the slope.

From Fig. 2, we see that the system crosses from the E_1 to E_3 states at about 290 T, where the magnetization changes. This theoretical result is consistent with the experiment [17] in which a two-step magnetization curve is obtained. However, a quantitative comparison between the theory and the measured data is not possible, because hysteretic effects are not reported and we are unable to locate the critical fields in equilibrium.

Since the experimental value of λ of Co^{3+} ion is not known, we treat it as an adjustable parameter together with δ and ε. Dunn has estimated the value of the one-electron spin-orbit coupling parameter ζ_{nd} by the use of extrapolation methods [18]. For Co^{3+}, $\zeta_{nd} = 580$ cm^{-1}, which gives for the ^5D state

$$\lambda = -\zeta_{nd}/4 = -145 \text{ cm}^{-1}. \quad (22)$$

From Eqs. (11) and (22), we have $\lambda' = -290$ cm^{-1}. In this Letter, we have chosen $\lambda' = -410$ cm^{-1}, somewhat larger than -290 cm^{-1}.

Noguchi *et al.* [19] present a phenomenological energy level scheme to explain their electron spin resonance (ESR) data, in which an excited triplet state lies above a singlet ground state. Evidently, this is not consistent with the energy level scheme used here (Fig. 1), in which the first excited state is a doublet. Ropka and Radwanski [20] explain Noguchi *et al.*'s energy diagram by introducing a highly excited multiplet ^1I to ^5D. Normally, the effects of excited multiplets on the ground state are small and do not alter the energy level scheme [21].

We offer an alternative scenario that gives an excited triplet. In this Letter, we have assumed that Co^{III} and Co^{3+} coexist in LCO, the former of which is magnetically silent
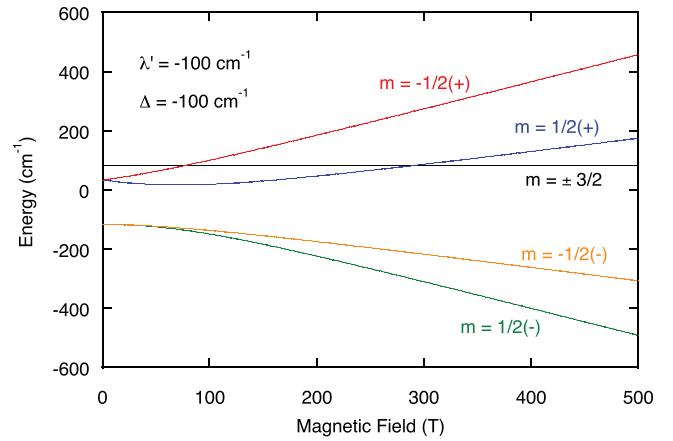

FIG. 4. The magnetic field dependence of the 6 eigenvalues of the Hamiltonian [Eq. (23)] when $\lambda' = -100$ cm^{-1} and $\Delta = -100$ cm^{-1}. Here, m is the eigenvalue of $l_z + s_z$.

at low temperatures. Since the ESR measurement [19] was performed at temperatures between 20 and 70 K, we expect that a considerable amount of Co^{III} becomes magnetic. An elementary excitation from the LS state is to excite one electron from Γ_5 to Γ_3. This results in a configuration in which one hole exists at Γ_5 and one electron at Γ_3. We note that the level splitting is reversed for the hole, i.e., Γ_5 lies higher than Γ_3. Here, we discuss the hole state with the following Hamiltonian,

$$\mathcal{H}_{\text{hole}} = -\lambda' \boldsymbol{l} \cdot \boldsymbol{s} - \Delta \left(l_z^2 - 2/3 \right) + \mu_B H (2s_z - l_z), \quad (23)$$

where s is the spin angular momentum of magnitude $\frac{1}{2}$. For simplicity, we consider the case of a tetragonal crystal field.

Similarly to the preceding discussion, we obtain 6 eigenvalues of Eq. (23) with $m = \pm\frac{3}{2}$ and $m = \pm\frac{1}{2}$. Note that each of the $m = \pm\frac{1}{2}$ has two values. Therefore, a quartet ($m = \pm\frac{3}{2}$ and $m = \pm\frac{1}{2}$) and a doublet ($m = \pm\frac{1}{2}$) exist as shown in Fig. 4. A relative position between the quartet and doublet depends on the spin-orbit interaction and the crystal field. From a simple calculation, it is shown that the quartet lies above the doublet for $(\Delta - 3\lambda'/2)^2 + 2\lambda'\Delta > 0$.

Figure 4 shows the 6 eigenvalues as a function of the applied magnetic field. We see an upper quartet and a lower doublet. Since the energy levels with $m = \pm\frac{3}{2}$ do not depend on magnetic field, the quartet is regarded as a quasitriplet. ESR transitions are possible between two states with $\Delta m = \pm 1$. Several ESR signals are expected to be observed between the energy levels shown in Fig. 4. A quantitative comparison between the experimental results will be made elsewhere.

The experimental evidence that the concentration of Co^{3+} in LCO changes with temperature [15] complicates the analysis of the $\chi(T)$ data. This will be discussed elsewhere.

In summary, it is shown that magnetization data on LCO conform to an intermediate crystal field model with trigonal symmetry. Satisfactory agreement between theory and available measurements is achieved with plausible values of the parameters, which include a spin-orbit interaction.

[1] Y. Kobayashi, K. Sato, and K. Asai, in *Spin-Crossover Phenomena in Perovskite Cobaltites: Their History and Current Status of the Research*, edited by Y. Okimoto, T. Saitoh, Y. Kobayashi, and S. Ishihara, Springer Series in Materials Science Vol. 305 (Springer, Singapore, 2021).

[2] R. R. Heikes, R. C. Miller, and R. Mazelsky, Physica **30**, 1600 (1964).

[3] M. A. Seńaris-Rodriguez and J. B. Goodenough, J. Solid State Chem. **116**, 224 (1995).

[4] M. Itoh, M. Sugahara, I. Natori, and K. Motoya, J. Phys. Soc. Jpn. **64**, 3967 (1995).

[5] A. Abragam and B. Bleaney, *Electron Paramagnetic Resonance of Transition Ions* (Oxford University Press, Oxford, UK, 1970).

[6] K. Inomata and T. Oguchi, J. Phys. Soc. Jpn. **23**, 765 (1967).

[7] A. Abragam and M. H. L. Pryce, Proc. R. Soc. London, Ser. A **205**, 135 (1951).

[8] J. Kanamori, Prog. Theor. Phys. **17**, 177 (1957).

[9] R. J. Radwański and Z. Ropka, Solid State Commun. **112**, 621 (1999).

[10] N. Menyuk, K. Dwight, and P. M. Raccah, J. Phys. Chem. Solids **28**, 549 (1967).

[11] C. L. Bull and K. S. Knight, Solid State Sci. **57**, 38 (2016).

[12] K. Sato, A. Matsuo, K. Kindo, Y. Kobayashi, and K. Asai, J. Phys. Soc. Jpn. **78**, 093702 (2009).

[13] The data extraction has been done using the software WebPlotDigitizer.

[14] J. B. Goodenough, J. Phys. Chem. Solids **6**, 287 (1958).

[15] V. G. Bhide, D. S. Rajoria, G. R. Rao, and C. N. R. Rao, Phys. Rev. B **6**, 1021 (1972).

[16] J. H. van Vleck, *The Theory of Electric and Magnetic Susceptibilities* (Oxford University Press, London, 1932).

[17] V. V. Platonov, Y. B. Kudasov, M. P. Monakhov, and O. M. Tatsenko, Phys. Solid State **54**, 279 (2012).

[18] T. M. Dunn, Trans. Faraday Soc. **57**, 1441 (1961).

[19] S. Noguchi, S. Kawamata, K. Okuda, H. Nojiri, and M. Motokawa, Phys. Rev. B **66**, 094404 (2002).

[20] Z. Ropka and R. J. Radwanski, Phys. Rev. B **67**, 172401 (2003).

[21] A. Abragam and M. H. L. Pryce, Proc. R. Soc. London, Ser. A **206**, 173 (1951).